Chapter 8

Anisotropic 2-D modelling of magnetic data from the Southern Andes

Although the preferred magnetotelluric strike direction roughly matches the expected structural strike (figure 7.7), and although a regional skew of <0.3 for most of the impedance data (figure 7.6) seems to justify the above presented isotropic 2-D approach which for the most part manages to reproduce the *inverted* data (i.e. the transfer functions Z_{xy}, Z_{yx}, T_y, d_D, z_D), the uniform north deflection of local induction vectors at longer periods clearly evinces that within the study area, a dimensionality greater than (isotropic) 2-D is observed (see figure 5.8).
Whatever the 'true' conductivity distribution looks like, the dominant strike direction is given by the the enormous land–sea conductivity contrast. The geomagnetic north component T_x of the local tipper functions from the three field stations F06, FUT and JWS, which are roughly equally distant from the deep sea and comprise a N-S distance of ∼230 km, plotted side by side, especially at longer periods shows marginal lateral along strike variation (figure 8.1). This strongly suggests that the observation might be explainable by 2-D modelling including (at least) horizontally anisotropic structures with an anisotropy strike $\alpha \neq 0$ with respect to the structural strike.

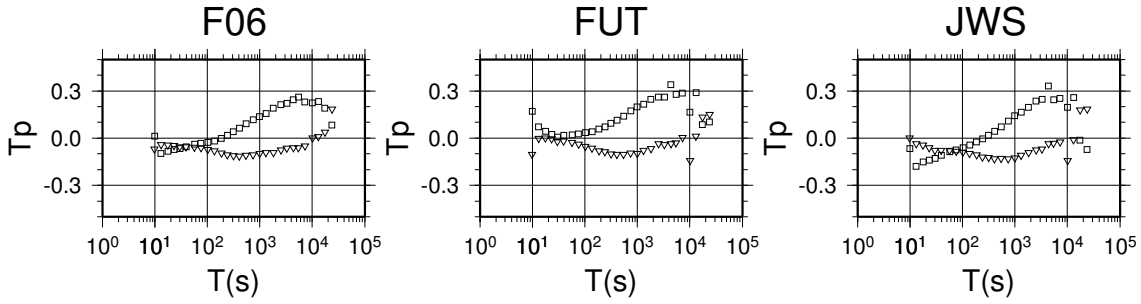

Figure 8.1: The geomagnetic north component T_x of local induction vectors (rectangles: real part, triangles: imaginary part) as a function of period comprises little change along strike (N-S distance between F06 and JWS: ∼230 km).

Having this concluded, an approach controlled by intuition which is based on experiences with isotropic structures will inevitably result in attempts to fit the data with anisotropy strikes roughly perpendicular to induction vectors. Model studies performed by *Pek and Verner* [1997], *Weidelt* [1999] and *Beike* [2001], however, make clear that this will work only in specific cases. Figure 8.2 qualitatively summarizes some results presented in *Pek and Verner* [1997] for simple 2-D conductivity distributions with anisotropic structures, which's anisotropy is equivalent to vertical conductive lamellae that are rotated by an anisotropy strike α. In cases where the 2-D contrast is based on a highly anisotropic structure itself, induction arrows are deflected against the direction of the preferred conductivity, as expected (model *a*). In contrast, if an isotropic 2-D conductor is coupled with an extended anisotropic body, induction arrows are rotated *into the anisotropy strike direction* (model *b* & *c*).

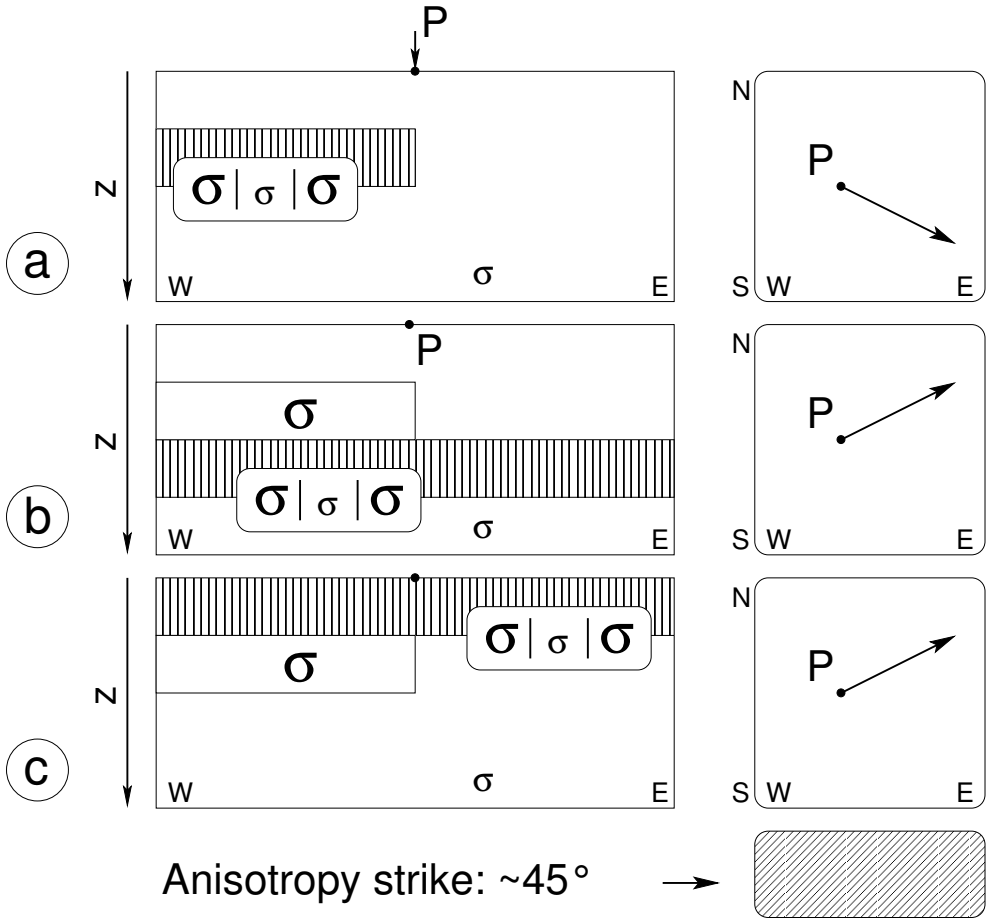

Figure 8.2: The deviation of local induction vectors at 2-D structures due to horizontal anisotropy of strike $\alpha > 0$, sketched from results of Pek and Verner [1997]. Left: side view on three 2-D models, all comprising anisotropic structures, which's anisotropy is equivalent with good conducting vertical lamellae, horizontally rotated by an angle α (patched structures). Sizes of the character σ reflect values of the respective (principal) conductivities. Right: Induction vectors at point P above the conductivity contrast. Vector deviations of model b and c are only qualitatively comparable, i.e. deviation is towards the same direction, but the effect is maximal at different periods.

Though at first glance rather surprising, this observation is indeed understandable. *Pek and Verner* [1997] presented plots of horizontal current densities for both polarizations, calculated for a model as given in figure 8.2c. For an inducing regional (concerning the structural strike) TE-polarization, the deflection of currents towards west (i.e. left) in the anisotropic layer does not entail a significant current density component perpendicular to the structural strike in the isotropic layer below. The northward deflection of currents in the anisotropic overburden, which is excited by an inducing regional TM-polarization, however, leads to a strong south component of the currents within the isotropic conductor. The clue to the understanding of this phenomenon is to regard the fields of the secondary currents, that are induced in the anisotropic structure by an inducing regional TM-polarization, as inducing fields that are incident on the isotropic conductor. The sketch in figure 8.3 illustrates this interpretation for the case of the 2-D contrast: anisotropic land with $\alpha > 0$ | (isotropic) sea. The onshore induced currents $\mathbf{j}^{\mathrm{I}}_{aniso}$ are deflected by an angle $90° - \alpha$ towards the direction of the well-conducting lamellae. Due to the refraction law for currents

$$\frac{\sigma^{\mathrm{I}}_{\parallel}}{\sigma^{\mathrm{II}}} \approx \frac{j^{\mathrm{I}}_{\parallel}}{j^{\mathrm{II}}_{\parallel}} = \frac{\tan\beta}{\tan\alpha} \tag{8.1}$$

(for $\sigma_{\parallel} \gg \sigma_{\perp}$, cf. figure 8.3. Here, σ_{sea} is the conductivity of sea water, and $\sigma_{\parallel}$ is the preferred conductivity of the anisotropic half-layer), almost for any realistic conductivity of the well-conducting lamellae, the inducing secondary currents $\mathbf{j}^{\mathrm{II}}_{aniso}$ are strongly deflected towards the structural strike ($\sigma_{\parallel} \ll \sigma_{sea} \rightarrow \beta \ll \alpha$), and so do the oppositely directed induced currents in the ocean. The anomalous magnetic field of the latter currents then has a positive downward component onshore which can be observed far inland. Thus, an inducing TM-polarization here leads to a positive vertical magnetic field, which means that $T_x > 0$, respectively that induction arrows point northward. As this would just be the opposite for $\alpha < 0$, we can conclude, that if an anisotropic structure adjoining the Pacific ocean in south Chile accounts for the observed north deviation of induction arrows, then its strike is positive in a clockwise rotational sense.

From the above considerations, it can be concluded that the investigation of an obvious anisotropic structure close to the ocean only in terms of geomagnetic transfer functions is best undertaken by concentrating on the geomagnetic north component T_x of the induction arrows in a 2-D anisotropic modelling study.
Allowing for anisotropy, the conductivity σ becomes a tensor, which, on account of the demanded nonnegativity of the time-averaged specific energy dissipation $\frac{1}{2}\mathbf{E}^*\mathbf{j} = \frac{1}{2}\mathbf{E}^*\boldsymbol{\sigma}\mathbf{E}$, is positive semidefinite (in conductors positive definite), and as purely ohmic conduction is considered, symmetric (*Onsager* [1931]):

$$\boldsymbol{\sigma} = \begin{pmatrix} \sigma_{xx} & \sigma_{xy} & \sigma_{xz} \\ \sigma_{xy} & \sigma_{yy} & \sigma_{yz} \\ \sigma_{xz} & \sigma_{yz} & \sigma_{zz} \end{pmatrix} \tag{8.2}$$

Such a tensor can be represented by three principal values and three rotation angles, i.e. from any coordinate system, the tensor can be transformed into diagonal form by three successive rotations (principal axis transformation). Like for isotropic 2-D conductivity distributions, only currents along the structural strike contribute to the vertical magnetic field component.

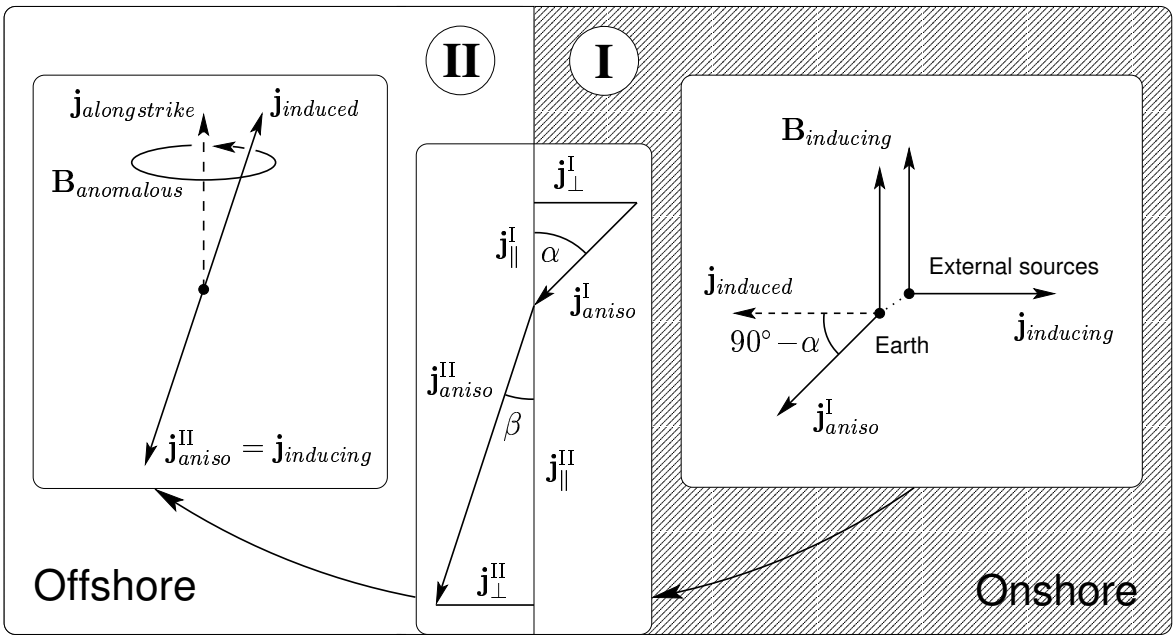

Figure 8.3: Sketch to explain the relation between B_z and B_x at a sea | anisotropic land contrast (after Weidelt [1999], modified for this specific setting). Onshore anisotropy is equivalent with well-conducting vertical lamellae of strike α. Secondary currents onshore, induced by an external magnetic field parallel to the strike direction, are deflected towards the better conducting direction (I). "Secondary secondary" currents, the ocean's response to from land incident secondary fields, due to the refraction at the structural border are mainly oriented along strike. Note that only the along strike component of the currents contributes to an anomalous magnetic field at the earth's surface, which is positive downward on land. The total *current density in the ocean results in a current flow in north-west direction.*

The here employed finite difference code from *Pek and Verner* [1997] calculates responses of 2-D conductivity distributions with arbitrary anisotropy for any element of the model (see there for any details on the code). Thus the model space increases by a factor of 6. Above horizontally anisotropic structures with an anisotropy strike diverging from the structural strike, a complete set of transfer functions for one station comprises eight (e.g., $\mathbf{Z}$, T_x, T_y, d_H, d_D — h_H & h_D are zero as $\partial B_x/\partial y = 0$ due to $\sigma_{air} = 0$ in equation 2.5c) instead of four (e.g., Z_{xy}, Z_{yx}, T_y, d_D) complex transfer functions (see also section 6.1.1), which means that the amount of data to be in principle modelled increases by a factor of 2.

In the modelling, only the horizontal strike angle α, which is the rotation angle by which the system of principal axes is rotated around the vertical axis with regard to the structural strike direction (which is here ∼N9°E), has been allowed to be unequal zero. Therefore, the principal conductivities will be referred to in the following with $\sigma_\parallel$, $\sigma_\perp < \sigma_\parallel$ (both in horizontal direction) and σ_z:

$$\boldsymbol{\sigma} = \begin{pmatrix} \sigma_\parallel \cos^2\alpha + \sigma_\perp \sin^2\alpha & (\sigma_\parallel - \sigma_\perp)\sin\alpha\cos\alpha & 0 \\ (\sigma_\parallel - \sigma_\perp)\sin\alpha\cos\alpha & \sigma_\parallel \sin^2\alpha + \sigma_\perp \cos^2\alpha & 0 \\ 0 & 0 & \sigma_z \end{pmatrix} \tag{8.3}$$

The models are discretized by 158 rows and 61 columns plus 10 air layers for the TE-mode. Sea water conductivity has been set to 0.27 Ωm. The shape of the subducting Nazca plate is deduced from hypocenter locations of recently recorded local earthquake data (*Bohm et al.* [2002]).

When modelling anisotropic structures, if additionally a reduced data set of just one type of transfer function is modelled, it is particularly difficult to be sure that the range of models has been exploited sufficiently. Still, it has been found that the data could only be explained by models of the *type* shown in figure 8.4. The only anisotropic structure of these models is a continental layer with an upper boundary in the mid crust and the integrated conductivities $\tau_{\|} \approx 800\,\mathrm{S}$ and $\tau_{\perp} \lesssim \tau_{\|}/30$. The anisotropy strike α is positive from geomagnetic north, somewhere between ∼15 and ∼60 degrees, best results have been obtained with $\alpha \approx 30°$. For this model, geomagnetic responses are completely insensitive to the vertical conductivity σ_z, so that $\sigma_z = \sigma_{\|}$ and $\sigma_z = \sigma_{\perp}$ yield comparable responses. This layer must be covered by an moderately conductive isotropic layer to ensure that $T_x \approx 0$ at short periods. Below the anisotropic layer, resistivities have to be high ($\gtrsim 1000\,\Omega\mathrm{m}$). Differing from the sketch described above, the anisotropic structure has no direct contact with the Pacific ocean, which is obviously not necessary to account for the phenomenon of along strike electrical currents in the ocean that are induced by an inducing regional TM polarization.

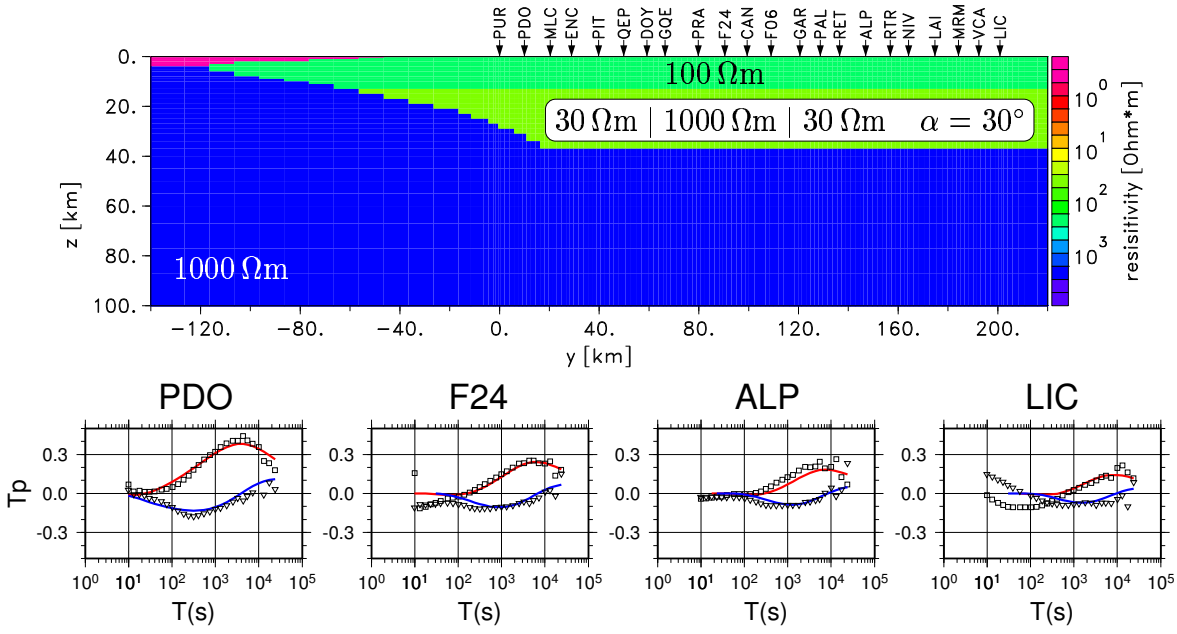

Figure 8.4: An anisotropic model for south Chile, which is preferred due to results from the isotropic 2-D modelling, and its response (T_x, i.e. the along strike component of induction vectors) from west to east at four stations (red: real parts, blue: imaginary parts). Between 13 km and 37 km depth, the model comprises an anisotropic continental layer with anisotropy strike $\alpha = 30°$ with respect to the structural strike, and the principal resistivities $\rho_{\|} = 30\,\Omega\mathrm{m}$, $\rho_{\perp} = 1000\,\Omega\mathrm{m}$ and $\rho_z = 1000\,\Omega\mathrm{m}$ (see text for discussion).

In figure 8.5, four alternative models with certain changes with regard to the 'preferred' model of figure 8.4 are shown. The thickness of the anisotropic layer in model *a* is reduced to a third (i.e. 8 km), while the principal conductivity $\sigma_{\parallel}$ is enhanced by a factor of three (i.e. 0.1 S/m), thus the integrated conductivity $\tau_{\parallel}$ being unchanged. The response of this model resembles that of the model in figure 8.4. In model *b*, the eastern part of the anisotropic layer is replaced by an isotropic conductor of 10 Ωm to account for the enhanced conductivities found there in the isotropic inversions of the previous section. This leads to an effect equivalent to the interaction anisotropic layer – ocean, but oriented in the other direction, opposing the former. In contrast, toward east increasing conductivities maintaining the anisotropy sustain the effect, making it even too strong (not illustrated; this is qualitatively a positive superposition of the effects shown in 8.2a and 8.2b,c). Surprisingly, decreased resistivities (here: 10 Ωm instead of 1000 Ωm) in the oceanic crust and *upper* oceanic lithosphere do not significantly change onshore responses (model *c*). If, however, the conductivity of the complete oceanic lithosphere is enhanced, responses are significantly smaller and shifted towards shorter periods (model *d*).

Some conclusions

Discovering electrical anisotropy from an analysis of geomagnetic variation data is bound to a lateral conductivity contrast which's strike does not match the anisotropy strike. The sharper the contrast, the stronger is the signature of anisotropy within the data. The enormous land–sea contrast, in isotropic electromagnetic respects clearly regarded as an obstruction, is thus an ideal environment for the discovery of continental anisotropy, particularly at active continental margins, where tectonic forces presumably accounting for anisotropy are especially high.

The disagreement of the anisotropic modelling with the isotropic modelling presented in section 7.4 is obvious. Also, the component of the induction vector perpendicular to the structural strike is not explained by this modelling. It is suggested, that results from both approaches reflect important aspects of the true conductivity distribution, and the task of further, necessarily anisotropic 2-D and/or 3-D modelling is to deduce *one* electrical image of the subsurface that is consistent with all types of data, impedance and pure geomagnetic transfer functions (see section 10).

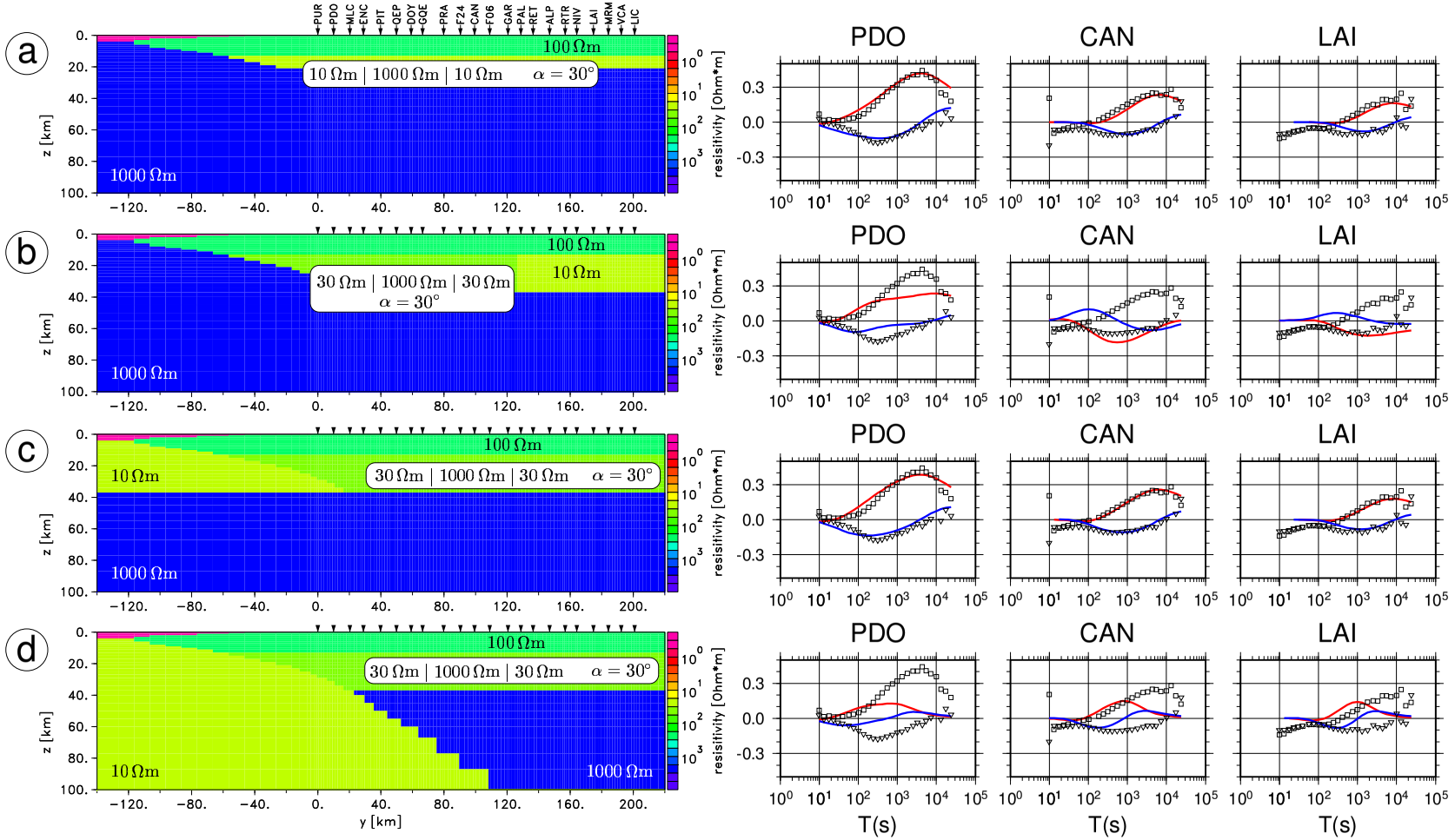

Figure 8.5: Four anisotropic 2-D models for the southern Andes, each with specific changes from the 'preferred' model in figure 8.4, and its responses (along strike component T_x of induction vectors at three selected stations from west to east). Resistivities in the round boxes refer to the principal resistivities $\sigma_{\parallel}$, $\sigma_{\perp}$ and σ_z. In all models, the anisotropy strike α is 30 degrees.